# **Relativistic Asymmetric Magnetic Reconnection**

#### Rostom Mbarek®\*

Department of Astronomy and Astrophysics, University of Chicago, Chicago, Illinois 60637, USA; Kavli Institute for Cosmological Physics, The University of Chicago, Chicago, Illinois 60637, USA and Enrico Fermi Institute, The University of Chicago, Chicago, Illinois 60637, USA

## Colby Haggerty

Institute for Astronomy, University of Hawai'i, Honolulu, Hawaii 96822, USA and Department of Astronomy and Astrophysics, University of Chicago, Chicago, Illinois 60637, USA

### Lorenzo Sironi

Department of Astronomy and Columbia Astrophysics Laboratory, Columbia University, New York, New York 10027, USA

### Michael Shay

Bartol Research Institute, Department of Physics and Astronomy, University of Delaware, Newark, Delaware 19716, USA

#### Damiano Caprioli

Department of Astronomy and Astrophysics, University of Chicago, Chicago, Illinois 60637, USA and Enrico Fermi Institute, The University of Chicago, Chicago, Illlinois 60637, USA

(Received 17 September 2021; revised 30 December 2021; accepted 11 March 2022; published 6 April 2022)

We derive basic scaling equations for relativistic magnetic reconnection in the general case of asymmetric inflow conditions and obtain predictions for the outflow Lorentz factor and the reconnection rate. Kinetic particle-in-cell simulations show that the outflow speeds as well as the nonthermal spectral index are constrained by the inflowing plasma with the weaker magnetic energy per particle, in agreement with the scaling predictions. These results are significant for understanding nonthermal emission from reconnection in magnetically dominated astrophysical systems, many of which may be asymmetric in nature. The results provide a quantitative approach for including asymmetry on reconnection in the relativistic regime.

DOI: 10.1103/PhysRevLett.128.145101

Introduction.—Magnetic reconnection is a fundamental plasma process through which energy stored in magnetic fields is converted into thermal and nonthermal particle energy. This process is a candidate for explaining impulsive nonthermal emission from magnetically dominated astrophysical objects such as gamma-ray bursts (GRBs) [1,2], pulsar winds [3,4], and jets from active galactic nuclei [5,6]. As the magnetic energy density becomes larger than the rest mass energy density of the plasma, reconnection generates power law distributions of energetic (> MeV) leptons [7–10].

There have been significant efforts to understand the basics of relativistic reconnection including: (i) its dynamics and scaling [11-14], (ii) the rate at which magnetic energy is dissipated, i.e., the reconnection rate [15–17], and (iii) nonthermal particle acceleration [16,18-32]. These works have shown that relativistic reconnection efficiently accelerates nonthermal particles. However, such studies have assumed that the magnetic field strength, temperature, and density of the reconnecting plasma regions are equal (symmetric case). Nevertheless, systems in which the inflowing parameters differ, i.e., asymmetric reconnection, is not an odd or rare event, with in situ observations of asymmetric reconnection frequently reported in the heliosphere [33–37]. Because of the prevalence of asymmetric reconnection in near-Earth systems, asymmetric reconnection has been thoroughly detailed [38-41]. Albeit extensive, this body of work is limited to nonrelativistic systems, and, presently, the description for asymmetric reconnection has not been extended to relativistic plasma, i.e., systems where the magnetic energy density is larger than the rest mass energy density of the plasma. The ubiquity of asymmetric reconnection in the heliosphere suggests that asymmetric reconnection can be as important to astrophysical environments. Likely examples include the boundary layer between the jet and accretion flow in active galactic nuclei (AGN) or shear flow boundaries warped by Kelvin-Helmholtz instabilities in AGN jets [4,6,42].

With this in mind, we present the first step in understanding asymmetric reconnection in the relativistic regime. We derive basic scaling predictions for relativistic asymmetric reconnection which reproduce both the symmetric relativistic and nonrelativistic asymmetric limits. We show that for asymmetric inflow density and magnetic fields, the reconnection rate and the outflow speed are set by the inflow with the weaker ratio of magnetic energy density to rest mass energy density, i.e., the magnetization  $\sigma$ . The predictions are tested with a survey of two-dimensional (2D) particle-in-cell (PIC) simulations, and show good agreement. Finally, we examine the effects of inflowing asymmetry on nonthermal particle acceleration, and show that the efficiency of particle acceleration is again controlled by the weaker-magnetization region.

Scaling of asymmetric reconnection.—If reconnection is occurring at a steady state, the characteristics of the outflowing plasma can be related to the inflowing properties by enforcing the conservation of mass and energy around a given X line. (Note that the conservation of momentum flux only provides a pressure balance constraint, and does not connect the inflow properties to the outflow one.) To this end, we consider an asymmetric diffusion region, with two distinct plasmas flowing in from below and above the current sheet; each with its own density and magnetic field strength flowing into a side with length L and with bulk velocities  $v_1$  and  $v_2$  (the 1 and 2 subscripts denote the distinct regions below and above the current sheet, respectively). The two populations mix as the magnetic energy is dissipated and the plasma is accelerated out of either side of the diffusion region with width  $\delta$ . For simplicity, we assume that the temperature of the inflowing plasma is nonrelativistic and the inflowing magnetic fields are antiparallel, i.e., the guide field is negligible.

The field on both sides of the current sheet is characterized by the magnetization, defined in this Letter as  $\sigma \equiv B'^2/4\pi\rho'c^2$ , where B' is the magnetic field strength,  $\rho'$  is the mass density, and c is the speed of light. Note that throughout the Letter, unless otherwise stated, unprimed variables are measured in the X line (or simulation) frame and primed variables are measured in the rest frame, i.e., the frame comoving with the fluid velocity v with Lorentz factor  $\gamma = 1/\sqrt{1-(v/c)^2}$ .

The equation governing the conservation of mass in the *X*-line frame is

$$L(\gamma_1 \rho_1' v_1 + \gamma_2 \rho_2' v_2) = 2\gamma_{\text{out}} \rho_{\text{out}}' v_{\text{out}} \delta. \tag{1}$$

The conservation of energy density flux [43,44] yields

$$\begin{split} L \left[ \left( w_1' + \frac{B_1'^2}{4\pi} \right) \gamma_1^2 v_1 + \left( w_2' + \frac{B_2'^2}{4\pi} \right) \gamma_2^2 v_2 \right] \\ &= 2\delta \left( w_{\text{out}}' + \frac{B_{\text{out}}'^2}{4\pi} \right) \gamma_{\text{out}}^2 v_{\text{out}}, \end{split} \tag{2}$$

where  $w' = \rho' c^2 + \Gamma P'_0/(\Gamma - 1)$  is the enthalpy density,  $\Gamma$  is the adiabatic index of the plasma, and P' is the pressure. We take the reconnection region to be in steady state and

apply Stokes's theorem to Faraday's law to obtain  $\vec{\nabla} \times \vec{E} = 0$ ; as a result, the inductive electric field driving reconnection  $E_z$  is uniform. The inflowing velocities are expressed as  $v_i/c = |\vec{E} \times \vec{B}_i|/B_i^2 \approx E/B_i$ , implying that  $\gamma_1 v_1 B_1' = \gamma_2 v_2 B_2'$ , since  $E_z$  is the same on both sides of the current sheet.

Using these considerations, assuming that  $B'_{out}$  is negligible compared to  $B'_1$  and  $B'_2$ , and dividing Eq. (2) by Eq. (1), we obtain,

$$\left(1 + \frac{\Gamma P_{\text{out}}'}{(\Gamma - 1)\rho_{\text{out}}'c^2}\right)\gamma_{\text{out}} = \frac{\gamma_1(1 + \sigma_1) + \xi\gamma_2(1 + \sigma_2)}{1 + \xi}, \quad (3)$$

where  $\xi \equiv (B_1' \rho_2'/B_2' \rho_1') = \sqrt{(\sigma_1 \rho_2'/\sigma_2 \rho_1')}$  and the inflowing initial temperatures are assumed to be nonrelativistic,  $w_{1,2}' \approx \rho_{1,2}' c^2$ . This equation provides a prediction for the Lorentz factor of the outflowing plasma  $\gamma_{\text{out}}$ , provided we know the outflowing pressure and density. Previous works on the scaling of reconnection have made diverging assumptions about the role of the thermal pressure in the exhaust: some works have assumed the pressure is negligible compared to the outflowing bulk kinetic energy density [13,38], while others take the pressure to be relativistically hot and comparable to the outflowing energy density [12,30]. For completeness, in this work we present both cases and show that simulations agree with the hot exhaust scenario.

In the limit of negligible pressure in the exhaust,  $w'_{\rm out} \approx \rho'_{\rm out}c^2$ , i.e., the magnetic energy is fully utilized to accelerate the plasma, Eq. (3) becomes

$$\gamma_{\text{out}} = \frac{\gamma_1(1+\sigma_1) + \gamma_2 \xi(1+\sigma_2)}{1+\xi}.$$
 (4)

This equation can be verified by considering the limiting behavior. For the symmetric relativistic case, as  $\sigma_1 = \sigma_2 = \sigma_{\rm in}$  and  $\xi \to 1$ , Eq. (4) becomes  $\gamma_{\rm out} \approx \gamma_{\rm in}(1+\sigma)$ , identical to the super-Alfvénic prediction in Lyutikov and Uzdensky [44]; in the nonrelativistic limit, we obtain the familiar  $v_{\rm out} \sim v_A = B_{\rm in}/\sqrt{4\pi\rho_{\rm in}}$ . Next, we consider the nonrelativistic asymmetric limit. Expanding Eq. (4) in the  $v_{\rm out} \ll c$  limit, we find  $v_{\rm out}^2 \approx 2c^2(\sigma_1 + \xi\sigma_2)/(1+\xi)$ , which can be rewritten in terms of the magnetic fields and densities:  $v_{\rm out}^2 \approx B_1 B_2/(2\pi\rho_{\rm tot})$ , where  $\rho_{\rm tot} = (\rho_1 B_2 + \rho_2 B_1)/(B_1 + B_2)$ , in agreement with the well-established predictions for nonrelativistic asymmetric outflows [45,46].

In the alternative case, in which the outflowing pressure is much larger than the rest mass energy density and cannot be neglected in the scaling derivation, an expression is needed for the exhaust pressure. In nonrelativistic magnetic reconnection, the energy per particle in the bulk flow is found to be comparable with the exhaust temperature in simulations, observations and experiments [37,47–51]. Motivated by this and by results from the simulations

preformed for this work, the exhaust pressure is taken to be,  $P'_{\rm out} \sim \rho'_{\rm out} \gamma_{\rm out} v^2_{\rm out} \sim \rho'_{\rm out} \gamma_{\rm out} c^2$ , and in this limit, the left-hand side of Eq. (3) is equal to  $4\gamma^2_{\rm out}$ , where we have used the relativistic adiabatic index of  $\Gamma=4/3$ . Applying this to Eq. (3) yields

$$\gamma_{\text{out}} \approx \sqrt{\frac{\gamma_1(1+\sigma_1) + \gamma_2\xi(1+\sigma_2)}{4(1+\xi)}}.$$
(5)

Taking this equation in the symmetric case, we recover the scaling relation of  $\gamma_{\rm out} \propto \sqrt{\sigma}$ , consistent with the Alfvénic outflow predictions of Lyubarsky [12] and Liu *et al.* [16].

Next we consider the limiting behavior of Eq. (5) for  $\sigma_2 \gg \sigma_1 \gg T/mc^2$ . In this limit, balancing magnetic and thermal pressure requires that  $\rho_1'/\rho_2' \sim \sigma_2/\sigma_1$ ,  $B_2' \sim B_1'$  (hence  $\gamma_1 \sim \gamma_2$ ), and  $\xi \sim \sigma_1/\sigma_2 \ll 1$ , the prediction for the outflowing Lorentz factor [Eq. (5)] becomes

$$\gamma_{\text{out}} \sim \frac{\sqrt{\gamma_1(1+2\sigma_1)}}{2}.$$
 (6)

Thus, for  $\sigma_2 \gg \sigma_1$ , the outflow speed is set by the weaker- $\sigma$  side, or, equivalently, the larger density side. This prediction should hold for both relativistic and non-relativistic values of  $\sigma_1$ .

Finally, we can use the outflow prediction to estimate the reconnection rate  $R \equiv v_1/v_{\rm out}$ , which is  $\approx v_2/v_{\rm out}$ , for systems where the upstream thermal energy is much smaller than the magnetic energy per particle. In such systems,  $v_1 \sim v_2$  since  $B_2' \sim B_1'$  and  $\xi \sim \sigma_1/\sigma_2$ , and hence, we can rewrite Eq. (1) in terms of the reconnection rate. In the limit where the inflow velocity is not ultrarelativistic ( $\sigma < 100$  and  $\gamma_{\rm in} \gtrsim 1$ ), we find an approximation for the asymmetric reconnection rate by taking the exhaust density as  $\rho_{\rm out} \sim (\rho_1 + \rho_2)/2$  following Cassak and Shay [46]:

$$R \approx \frac{\delta}{2L} \sqrt{1 + \frac{2\sigma_1 \sigma_2}{\sigma_1 + \sigma_2}}. (7)$$

This prediction is again only valid for mildly relativistic cases ( $\gamma_{\rm in} \gtrsim 1$ ); nevertheless, considering that the weaker- $\sigma$  side sets the reconnection rate, such a scaling is pertinent for asymmetric environments with  $\min(\sigma_1, \sigma_2) \lesssim 100$ , and consequently for symmetric environments with  $\sigma \lesssim 100$ .

Simulation setup.—To test the scaling predictions outlined above, we perform 2.5D (2D real space, 3D velocity space) particle-in-cell (PIC) simulations of electron-positron (pair-plasma) reconnection with TRISTAN-MP [52,53]. The plasma is comprised of electron-positron pairs, typical of high-energy astrophysical environments such as pulsar winds and AGN jets [54,55]. Both electrons and positrons are initialized with a constant temperature,  $\Delta \gamma \equiv k_B T'/mc^2 = 0.25$ . Throughout the simulations, no notable differences between electron and positron properties are observed.

Initializing a single stable current sheet in the simulations requires balancing pressure across the current sheet; and thus the density and magnetic field on the two sides are uniquely determined for a fixed temperature and a particular combination of  $\sigma_1$  and  $\sigma_2$ . (The ratio of the magnetic fields across the exhaust is given by  $B_2'/B_1' = \sqrt{(1+4\Delta\gamma/\sigma_1/1+4\Delta\gamma/\sigma_2)}$ .) Note that pressure balance stipulates that the magnetic field is roughly similar across the sheet if the initial temperature is relatively low as discussed above. For additional details on the simulations, the setup and the normalization see the Supplemental Material [56].

Simulation results.—We study relativistic asymmetric reconnection by performing a survey of simulations where the upper magnetization scans between  $\sigma_2 = 10^{-1}$  and  $10^3$ ; the lower is fixed at  $\sigma_1 = 10$ . Figure 1 compares the mass density  $(\rho)$  and outflow velocities  $(v_x)$  for the  $\sigma_2 = 10$  case (i.e., symmetric) and the  $\sigma_2=0.25$  case (i.e., asymmetric), at  $t\omega_p \approx 400$  for positrons. Note, that for the latter asymmetric case the assumption  $\sigma_2 \gg T/mc^2$  is not satisfied; however, we include this limit to show the effect two reconnecting regions with  $\sigma$ 's that differ by orders of magnitude. The most notable difference between the symmetric and asymmetric cases is the shape of the exhaust that morphs from round islands to a more elongated shape, preferentially protruding into the inflow region with the weaker magnetic field strength because it has a faster inflow velocity. The island bulges into this side to replace the higher volume of plasma that has reconnected [46,57]. Additionally, more plasmoids are present in the symmetric

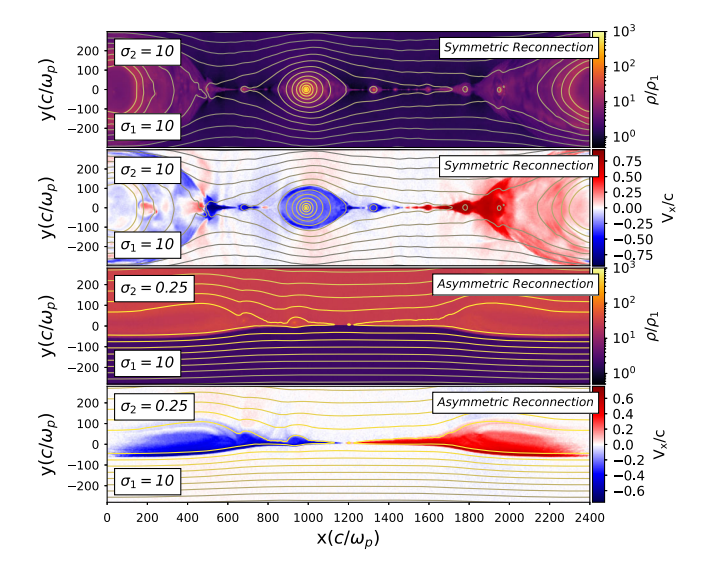


FIG. 1. Reconnection layer at  $t\omega_p \sim 400$  for both symmetric and asymmetric reconnection. The magnetization  $\sigma$  is specified in the plot on both sides of the current sheet. Contour maps of the magnetic scalar potential are also shown for reference. Top panels: Mass density map normalized to the mass density in the lower region  $\rho_1$ . Bottom panels: Outflow speed  $v_x$  in units of c.

simulation compared to the asymmetric case, which may be due to a combination of the apparent broader asymmetric exhaust and the documented reduction of plasmoids for weaker  $\sigma$  in symmetric reconnection [58]. Finally, the area of the islands suggest that less magnetic flux has been reconnected in the asymmetric simulation, consistent with the scaling predictions associated with Eq. (5). For the  $\sigma_2 \gg \sigma_1$  case (not shown), the shape of the exhaust looks similar to symmetric reconnection, with the island expanding both inflow regions equally.

To further verify the scaling predictions, the reconnection rates in the survey of symmetric and asymmetric simulations are measured and shown in Fig. 2 as a function of  $\sigma_2$ . The teal dots and crosses show  $v_{\rm in}/v_{\rm out}$ , where  $v_{\rm out}$  is a spatially averaged absolute value in the center of the exhaust  $(y \sim 0)$  and  $v_{in}$  is the absolute value of the average of both sides within  $5c/\omega_p$  away from the X line in the inflow region. The blue dots and crosses show a similar value, but with the outflow velocity assumed to be c (appropriate for  $\sigma_1, \sigma_2 \gg 1$ ); The dashed green line shows the prediction for the reconnection rate from Eq. (5) of Liu et al. [16]. [For Eq. (3) from Liu et al. [16], we use  $r_{n'}\delta/L = 0.1$  and include the thermal contribution to enthalpy with  $k_B T' = mc^2/4$ .] The black dashed and solid lines show the expected reconnection rate based on Eq. (7) for  $\delta/L = 0.15$  (the best fit for our simulation results), which is comparable with Liu et al.'s [16] favored aspect ratio. Finally, the edges of the corresponding shaded regions are defined by the values measured on either upstream regions, e.g., the upper extent will be the average reconnection rate determined from the upper half of the

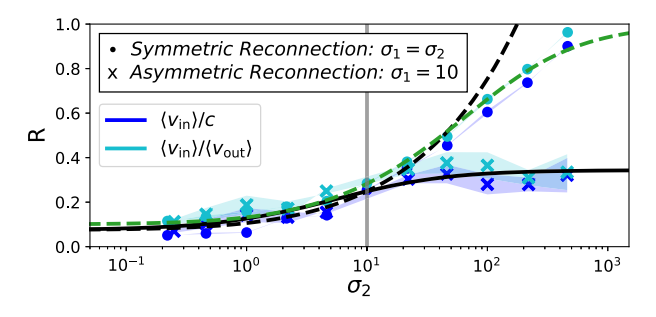


FIG. 2. Reconnection rate for different magnetization parameters in simulations of symmetric and asymmetric cases. The green dashed curve shows the expected symmetric reconnection rate based on the prediction of Liu *et al.* [16], including the plasma thermal pressure. The teal and blue dots (crosses) show the averaged measured values of  $\langle v_{\rm in} \rangle$  normalized to  $\langle v_{\rm out} \rangle$  and c, respectively, for symmetric (asymmetric) reconnection. The averages are determined over a  $5d_e$  window just upstream of the X line. The black dashed (solid) line shows the prediction for the for symmetric (asymmetric) reconnection rate determined by Eq. (7); such a prediction is only valid for environments with  $\min(\sigma_1,\sigma_2)\lesssim 100$  as explained in the text. For the asymmetric cases,  $\sigma_1=10$  is fixed and the reconnection rate is controlled by the weaker  $\sigma$ .

current sheet ( $\sigma_2$  region) and the lower extent of the shaded region will be the averaged value below the current sheet ( $\sigma_1$  region). Considering that  $v_1 \sim v_2$  for small values of  $k_B T/mc^2 \ll \sigma_1, \sigma_2$ , we expect the shaded regions to have a limited extent especially as  $\sigma_2 \to \sigma_1$ . The simulation measurements were taken at  $400\omega_p^{-1}$ . This is not the longest timescale for all runs, but we choose this time as a representative steady-state snapshot, well after reconnection has started, but before island size inhibits efficient reconnection.

Symmetric simulations in Fig. 2 yield results consistent with predictions from previous studies; the reconnection rate increases from the standard nonrelativistic 0.1 value, up to almost nearly 1 for simulations with  $\sigma \gg 1$  [14,16]. For the asymmetric simulations,  $\sigma_1$  is fixed to 10 and  $\sigma_2$  is varied over ~4 orders of magnitude. For the asymmetric simulations, the reconnection rates are set by the weaker- $\sigma$ regions. For  $\sigma_2 < \sigma_1$ , asymmetric reconnection rates are comparable to the symmetric  $\sigma_2$  counterparts, and for  $\sigma_2 > \sigma_1$ , the rate becomes insensitive to increases in  $\sigma_2$ . This can primarily be attributed to the exhaust field lines becoming mass loaded by the weaker  $\sigma_1$  (i.e., larger density) inflow. From these considerations, our simulations verify that the reconnection rate is quenched by the side of the exhaust with the weaker magnetization parameter, as predicted by Eq. (6), even in the extreme limit where  $n_2' \to 0$  or vacuum, i.e.,  $\sigma_2 \to \infty$  (as shown in the Supplemental Material [56]).

Nonthermal particle spectra.—To examine particle acceleration, we show the energy distribution functions in Fig. 3 for different symmetric and asymmetric conditions at different times, averaged over the entire domain, with the time stamp of representative distributions, color coded based on the color bar shade. We show the distributions for five different characteristic example simulations in Fig. 3 that exhibit nonthermal, extended tails reaching ultrarelativistic energies. The spectra with the red, blue, and green color correspond to  $\sigma_2 = 0.25$ , 10, and 100, respectively, with  $\sigma_1$  fixed to 10 and are fitted at  $t\omega_p \sim 450$  with a spectral slope  $q \equiv -d \log N/\log \gamma$ . We also show the spectra for the symmetric cases  $\sigma = 0.25$  and  $\sigma = 100$  (the purple and orange lines, respectively) at  $t\omega_p \sim 450$  with their power law fit.

Asymmetric simulations develop power-law spectral slopes between those of their symmetric counterparts. Following similar trends, we find that the spectra associated with  $\sigma_2=0.25$  (red curves) are much steeper than those with a symmetric  $\sigma=10$  prescription, and can conclude that a power law distribution essentially does not form. The symmetric  $\sigma=0.25$  case has the steepest distribution as expected.

The inset of Fig. 3 shows the power law slopes for symmetric and asymmetric ( $\sigma_1 = 10$  for asymmetric cases) simulations over a range of  $\sigma$ 's and exhibits the same trend for a range of different magnetizations. Overall, it appears

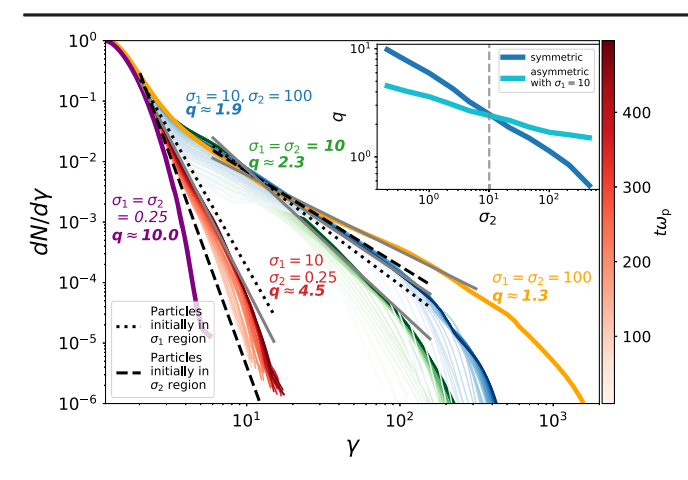


FIG. 3. Time evolution of particle energy spectra for symmetric and asymmetric reconnection with different magnetization parameters. The time stamp of each distribution is color coded based on the color bar shade for one representative example ( $\sigma_1 = 10$ ,  $\sigma_2 = 0.25$ ). The spectrum tends towards a power law slope as time progresses. The dashed and dotted lines show the best fit values for slopes of the power law spectra based on particles originating from the lower and upper inflow regions, respectively, while the gray solid lines show the best fit for the combined population. The upper right plot shows the dependence of the slope for different magnetization parameters for both symmetric and asymmetric reconnection.

from these simulations that for asymmetric reconnection, the accelerated particle spectra are steepened relative to the larger  $\sigma$  side, and hardened relative to the weaker  $\sigma$  side.

Finally, for spectra associated with asymmetric reconnection, we separately present the spectra of positrons coming from either the upper or lower half of the domain; dotted lines correspond to particles initialized on the lower half of the current sheet  $(\sigma_1)$ , and dashed lines for particles from the upper domain  $(\sigma_2)$ . We note that particles starting in the higher  $\sigma$  regions have a flatter slope and tend towards higher energies as can be seen in more detail in Fig. 3.

Conclusions.—In this Letter we present the first examination of relativistic, magnetic reconnection, with asymmetric inflowing conditions. We consider systems with asymmetric densities and magnetic fields but with a constant, nonrelativistic temperature for simplicity. Using conservation of mass and energy, we derive a scaling prediction for the outgoing bulk flow Lorentz factor, and show that the prediction is consistent with standard limiting cases. For systems with a large asymmetry in magnetization, the evolution of reconnection is determined by the smaller  $\sigma$  value (Fig. 2).

The predictions are tested using a survey of 2.5D fully kinetic particle-in-cell simulations performed with TRISTAN-MP [52,53]. The scaling relations are found to accurately predict the outflow and reconnection rate of simulations. We anecdotally find that asymmetric simulations generate less plasmoids than their symmetric counterparts.

We also consider the production of nonthermal particles in the simulations, finding that extended power-law distributions can be produced by asymmetric reconnection, with a slope that depends on the magnetization of both inflowing plasmas. Each asymmetric simulation develops a power-law distribution where the spectral slope falls between the slopes of the two symmetric counterparts.

While we anticipate these results to extend to fully 3D systems—as has been shown for the scaling in nonrelativistic simulations [59,60] and the acceleration in relativistic simulations [7,29]—it should be noted that reconnection in three dimensions is susceptible to other instabilities that can potentially affect the scaling properties and particle acceleration [61–63]. This work makes the first step towards understanding asymmetric relativistic magnetic reconnection, but future work is needed to characterize the full 3D nature of the problem.

Simulations were performed on computational resources provided by the University of Chicago Research Computing Center and XSEDE TACC (TG-AST180008). C. C. H. acknowledges support from NSF FDSS Grant No. AGS-1936393; L. S. acknowledges support from the Cottrell Scholars Award, NASA 80NSSC20K1556, NSF PHY-1903412, DoE DE-SC0021254, and NSF AST-2108201; D. C. acknowledges support from NASA Grant No. 80NSSC18K1218 and NSF Grant No. PHY-2010240, and M. S. acknowledges NSF Grant No. AGS-2024198 NASA Grant No. 80NSSC20K0198.

<sup>\*</sup>rmbarek@uchicago.edu

J. C. McKinney and D. A. Uzdensky, Mon. Not. R. Astron. Soc. 419, 573 (2012).

<sup>[2]</sup> B. Zhang and H. Yan, Astrophys. J. 726, 90 (2011).

<sup>[3]</sup> J. Arons, Space Sci. Rev. 173, 341 (2012).

<sup>[4]</sup> Y. Lyubarsky and J. G. Kirk, Astrophys. J. **547**, 437 (2001).

<sup>[5]</sup> D. Giannios, Mon. Not. R. Astron. Soc. 408, L46 (2010).

<sup>[6]</sup> L. Sironi, M. E. Rowan, and R. Narayan, Astrophys. J. 907, L44 (2021).

<sup>[7]</sup> F. Guo, H. Li, W. Daughton, and Y.-H. Liu, Phys. Rev. Lett. 113, 155005 (2014).

<sup>[8]</sup> F. Guo, Y.-H. Liu, W. Daughton, and H. Li, Astrophys. J. 806, 167 (2015).

<sup>[9]</sup> L. Sironi, M. Petropoulou, and D. Giannios, Mon. Not. R. Astron. Soc. 450, 183 (2015).

<sup>[10]</sup> G. R. Werner, D. A. Uzdensky, B. Cerutti, K. Nalewajko, and M. C. Begelman, Astrophys. J. Lett. **816**, L8 (2016).

<sup>[11]</sup> E. G. Blackman and G. B. Field, Phys. Rev. Lett. 72, 494 (1994).

<sup>[12]</sup> Y. E. Lyubarsky, Mon. Not. R. Astron. Soc. **358**, 113 (2005).

<sup>[13]</sup> M. Lyutikov, Mon. Not. R. Astron. Soc. 346, 540 (2003).

<sup>[14]</sup> H. R. Takahashi, T. Kudoh, Y. Masada, and J. Matsumoto, Astrophys. J. **739**, L53 (2011).

<sup>[15]</sup> M. Hesse, T. Neukirch, K. Schindler, M. Kuznetsova, and S. Zenitani, Space Sci. Rev. 160, 3 (2011).

- [16] Y.-H. Liu, F. Guo, W. Daughton, H. Li, and M. Hesse, Phys. Rev. Lett. 114, 095002 (2015).
- [17] S. Zenitani and M. Hoshino, Astrophys. J. **670**, 702 (2007).
- [18] D. Ball, L. Sironi, and F. Özel, Astrophys. J. **862**, 80 (2018).
- [19] N. Bessho and A. Bhattacharjee, Astrophys. J. 750, 129 (2012).
- [20] B. Cerutti, D. A. Uzdensky, and M. C. Begelman, Astrophys. J. 746, 148 (2012).
- [21] B. Cerutti, G. R. Werner, D. A. Uzdensky, and M. C. Begelman, Astrophys. J. 770, 147 (2013).
- [22] B. Cerutti, G. R. Werner, D. A. Uzdensky, and M. C. Begelman, Phys. Plasmas 21, 056501 (2014).
- [23] B. Cerutti, G. R. Werner, D. A. Uzdensky, and M. C. Begelman, Astrophys. J. 782, 104 (2014).
- [24] C. H. Jaroschek, H. Lesch, and R. A. Treumann, Astrophys. J. Lett. 605, L9 (2004).
- [25] D. Kagan, M. Milosavljević, and A. Spitkovsky, Astrophys. J. 774, 41 (2013).
- [26] D. Kagan, L. Sironi, B. Cerutti, and D. Giannios, Space Sci. Rev. 191, 545 (2015).
- [27] M. E. Rowan, L. Sironi, and R. Narayan, Astrophys. J. 850, 29 (2017).
- [28] L. Sironi and A. Spitkovsky, Astrophys. J. 741, 39 (2011).
- [29] L. Sironi and A. Spitkovsky, Astrophys. J. Lett. 783, L21 (2014).
- [30] S. Zenitani and M. Hesse, Astrophys. J. 684, 1477 (2008).
- [31] S. Zenitani and M. Hoshino, Astrophys. J. Lett. **562**, L63 (2001).
- [32] S. Zenitani and M. Hoshino, Astrophys. J. Lett. 618, L111 (2005).
- [33] J. L. Burch, R. B. Torbert, T. D. Phan, L. J. Chen, T. E. Moore, R. E. Ergun, J. P. Eastwood, D. J. Gershman, P. A. Cassak, M. R. Argall, S. Wang, M. Hesse *et al.*, Science 352, aaf2939 (2016).
- [34] R. Mistry, J. P. Eastwood, T. D. Phan, and H. Hietala, J. Geophys. Res. Space Phys. **122**, 5895 (2017).
- [35] M. Øieroset, T. D. Phan, and M. Fujimoto, Geophys. Res. Lett. 31, L12801 (2004).
- [36] G. Paschmann, M. Øieroset, and T. Phan, Space Sci. Rev. **178**, 385 (2013).
- [37] T. D. Phan, M. A. Shay, J. T. Gosling, M. Fujimoto, J. F. Drake, G. Paschmann, M. Oieroset, J. P. Eastwood, and V. Angelopoulos, Geophys. Res. Lett. **40**, 4475 (2013).
- [38] P. A. Cassak and M. A. Shay, Geophys. Res. Lett. 35, L19102 (2008).
- [39] K. Malakit, M. A. Shay, P. A. Cassak, and C. Bard, J. Geophys. Res. Space Phys. **115**, A10223 (2010).
- [40] M. A. Shay, T. D. Phan, C. C. Haggerty, M. Fujimoto, J. F. Drake, K. Malakit, P. A. Cassak, and M. Swisdak, Geophys. Res. Lett. **43**, 4145 (2016).
- [41] M. Swisdak, B. N. Rogers, J. F. Drake, and M. A. Shay, J. Geophys. Res. Space Phys. 108, 1218 (2003).
- [42] B. Ripperda, F. Bacchini, and A. A. Philippov, Astrophys. J. 900, 100 (2020).

- [43] A. Lichnerowicz, Relativistic Hydrodynamics and Magnetohydrodynamics (W.A. Benjamin, Inc., San Francisco, 1967).
- [44] M. Lyutikov and D. Uzdensky, Astrophys. J. 589, 893 (2003).
- [45] J. Birn, J. E. Borovsky, M. Hesse, and K. Schindler, Phys. Plasmas 17, 052108 (2010).
- [46] P. A. Cassak and M. A. Shay, Phys. Plasmas 14, 102114 (2007).
- [47] C. C. Haggerty, T. N. Parashar, W. H. Matthaeus, M. A. Shay, Y. Yang, M. Wan, P. Wu, and S. Servidio, Phys. Plasmas 24, 102308 (2017).
- [48] C. C. Haggerty, M. A. Shay, A. Chasapis, T. D. Phan, J. F. Drake, K. Malakit, P. A. Cassak, and R. Kieokaew, Phys. Plasmas 25, 102120 (2018).
- [49] T. Phan, J. Drake, M. Shay, J. Gosling, G. Paschmann, J. Eastwood, M. Øieroset, M. Fujimoto, and V. Angelopoulos, Geophys. Res. Lett. 41, 7002 (2014).
- [50] M. A. Shay, C. C. Haggerty, T. D. Phan, J. F. Drake, P. A. Cassak, P. Wu, M. Oieroset, M. Swisdak, and K. Malakit, Phys. Plasmas 21, 122902 (2014).
- [51] M. Yamada, J. Yoo, J. Jara-Almonte, W. Daughton, H. Ji, R. M. Kulsrud, and C. E. Myers, Phys. Plasmas 22, 056501 (2015).
- [52] O. Buneman, Computer Space Plasma Physics: Simulation Techniques and Software, edited by H. Matsumoto and Y. Omura (Terra Scientific, Tokyo, 1993), ISBN 9784887041110.
- [53] A. Spitkovsky, AIP Conf. Proc. 801, 345 (2005).
- [54] P. A. Sturrock, Astrophys. J. 164, 529 (1971).
- [55] J. F. C. Wardle, D. C. Homan, R. Ojha, and D. H. Roberts, Nature (London) 395, 457 (1998).
- [56] See Supplemental Material at http://link.aps.org/supplemental/10.1103/PhysRevLett.128.145101 for additional details on the simulations' setup and normalization, along with limiting cases.
- [57] D. Krauss-Varban, H. Karimabadi, and N. Omidi, Geophys. Res. Lett. 26, 1235 (1999).
- [58] L. Sironi, D. Giannios, and M. Petropoulou, Mon. Not. R. Astron. Soc. 462, 48 (2016).
- [59] W. Daughton, T. K. M. Nakamura, H. Karimabadi, V. Roytershteyn, and B. Loring, Phys. Plasmas 21, 052307 (2014).
- [60] T. C. Li, Y.-H. Liu, M. Hesse, and Y. Zou, J. Geophys. Res. Space Phys. 125, e27094 (2020).
- [61] L. Price, M. Swisdak, J.F. Drake, P.A. Cassak, J.T. Dahlin, and R.E. Ergun, Geophys. Res. Lett. 43, 6020 (2016).
- [62] H. Zhang, L. Sironi, and D. Giannios, Astrophys. J. 922, 261 (2021).
- [63] Q. Zhang, F. Guo, W. Daughton, H. Li, and X. Li, Phys. Rev. Lett. 127, 185101 (2021).